Supporting Information

Williams et al. 10.1073/pnas.1220240110

SI Materials and Methods

All manipulations of air- and moisture-sensitive compounds were carried out with rigorous exclusion of O_2 and moisture in flame- or oven-dried Schlenk-type glassware interfaced to a dual manifold Schlenk line, or to a high-vacuum (10^{-5}–10^{-6} Torr) line, or in an N_2-filled glovebox with a high-capacity recirculator (<1 ppm O_2). Argon (Airgas, prepurified) and H_2 (Airgas) were purified by passage through MnO/vermiculite and Davidson 4A molecular sieve columns. All hydrocarbon solvents (*n*-pentane, toluene, benzene) were transferred from Na/K alloy. Solution phase NMR spectra were recorded on either a Varian Inova-400 [Fourier Transform (FT), 400 MHz, ^{1}H; 100 MHz, ^{13}C] or an Inova-500 (FT, 500 MHz, ^{1}H; 125 MHz,^{13}C) spectrometer. Chemical shifts (δ) for ^{1}H and ^{13}C spectra were referenced using internal solvent resonances and are reported relative to tetramethylsilane. ^{1}H- and ^{13}C-NMR experiments on air-sensitive solution samples were conducted in Teflon valve-sealed sample tubes (J-Young). ^{13}C-cross-polarization magic angle spinning (CPMAS) solid-state NMR spectra were recorded on a Varian VXR400 (FT, 100 MHz, ^{13}C). For ^{13}C-CPMAS solid-state NMR spectroscopy, air-sensitive samples were loaded into cylindrical zirconia rotors in the glovebox and capped with a solid Teflon cap. For routine spectra of organozirconium adsorbates, the cross-polarization contact time was 2 ms and the recycle time was 5 s. For adsorbed complexes, 16,000 scans were required to obtain satisfactory signal:noise ratios, with a spinning rate of 5 kHz, depending on peak location vs. the location of spinning sidebands. Chemical shifts (δ) for ^{13}C-CPMAS solid-state NMR spectra are reported relative to the external methylene signal of adamantane (38.48 ppm) (1). For ^{13}C-CPMAS-NMR experiments, a solution of 10% (vol/vol) ^{13}C-enriched benzene in benzene was used. ^{13}C-enriched benzene was purchased from Cambridge Isotope Laboratories ($^{13}C_6$, 99%), dried over Na/K alloy, and stored in a sealed storage tube. Cp_2ZrH_2 (**A**) was purchased from Alfa Aesar, and used without further purification. Alumina was obtained from Alfa Aesar (γ-alumina, 99.97% metal basis), whereas $B(C_6F_5)_3$ and $[Ph_3C][B(C_6F_5)_4]$ were a generous gift from Albemarle Corp. The complexes $Cp_2Zr(CH_3)_2$ (**B**) (2), $Cp^*Zr(CH_3)_3$ (**C**) (3), and sulfated alumina (AlS) (4) were prepared by literature procedures.

Chemisorption of Organometallic Complexes on Sulfated Alumina. In a two-sided, flame-dried fritted reaction vessel interfaced to the high-vacuum line, 15 mL of pentane was condensed onto carefully measured quantities of the organometallic complex and support. The typical mass ratio of organometallic complex to support was 1:15. The resulting slurry was stirred at 25 °C for 1 h, then filtered. The impregnated support was collected on the frit and washed five times with pentane, then dried in vacuo for 1 h. The impregnated support was stored under dry N_2 at −40 °C until used.

Hydrogenolysis of $Cp^*Zr^{13}Me_3$/AlS. A 15-mL water-jacketed Morton flask reactor was charged in the glovebox with 400 mg of $Cp^*Zr^{13}Me_3$/AlS and 5.0 mL of dry pentane. The closed reactor was then removed from the glovebox, interfaced to the high-vacuum line, and freeze-pump-thaw degassed at −78 °C. The thermostated reactor was then equilibrated for 15 min at 25.0 (±1) °C and the flask agitated using a vortex mixer (2,000 rpm, Scientific Industries, Inc., Digital Vortex-Genie 2 Mixer, 120V, 60Hz) for 4 h under constant pressure of 1.0 atm of H_2. The volatiles were then removed in vacuo and the supported complex **C′/AlS** + H_2 was stored in a Teflon-sealed storage tube at 0 °C.

Dosing of Cp^*ZrMe_3/AlS with Benzene. A 15-mL Morton reactor flask was charged in the glovebox with 200 mg of Cp^*ZrMe_3/AlS and 5.0 mL of dry benzene (or 10% ^{13}C-enriched benzene in benzene). The closed reactor was then removed from the glovebox, interfaced to the vacuum line, and freeze-pump-thaw degassed. The thermostated reactor was then equilibrated for 15 min at 25.0 (±1) °C and the flask agitated using the aforementioned vortex mixer (2,000 rpm) for 4 h. The volatiles were then removed in vacuo and the benzene-dosed supported complex (**C·C_6H_6/AlS**) stored in a sealed storage tube at 0 °C.

Benzene Hydrogenation Experiment with Cp^*ZrMe_3/AlS. In a typical experiment, a 15-L water-jacketed Morton flask, dried overnight in a 160 °C oven, was charged in the glovebox with 50 mg of supported catalyst and 1.0 mL of dry substrate. The closed reactor was then removed from the glovebox, interfaced to the high-vacuum line, and freeze-pump-thaw degassed at −78 °C. The reactor was then connected to a thermostated circulating water supply and equilibrated for 15 min at 25.0 (±1) °C. Next, the flask was agitated using a vortex mixer (2,000 rpm), then pressurized to 1.0 atm of H_2. The reaction was monitored by ^{1}H-NMR spectroscopy, which indicated 250 μmol of cyclohexane was produced in 1 h (TOF = 120 mol C_6H_6·mol Zr·h^{-1}).

Benzene Hydrogenation Experiment with Cp^*ZrMe_3 + $B(C_6F_5)_3$. To a mixture of 10 mg (36.8 μmol) Cp^*ZrMe_3 and 20 mg (39.1 μmol) $B(C_6F_5)_3$ was added 2 mL (22 mmol) of benzene in the glovebox. The mixture immediately became a pale yellow solution. The reactor was removed from the glovebox and attached to the high-vacuum line. After thorough evacuation (10^{-5} Torr) of the reactor at −78 °C, the reactor was warmed to room temperature and pressurized to 1.0 atm of H_2. The mixture was then stirred rapidly at room temperature for 1 h. The reaction was monitored by ^{1}H-NMR spectroscopy, which indicated 53 μmol of cyclohexane was produced in 1 h (TOF = 1.4 mol C_6H_6·mol Zr·h^{-1}).

Benzene Hydrogenation Experiment with Cp^*ZrMe_3 + $[Ph_3C][B(C_6F_5)_4]$. To a mixture of 12 mg (44.1 μmol) Cp^*ZrMe_3 and 45 mg (48.8 μmol) $[Ph_3C][B(C_6F_5)_4]$ was added 2 mL (22 mmol) of benzene in the glovebox. The mixture immediately became a pale yellow solution. The reactor was removed from the glovebox and attached to the high-vacuum line. After thorough evacuation (10^{-5} Torr) of the reactor at −78 °C, the reactor was warmed to room temperature and pressurized to 1.0 atm of H_2. The mixture was then stirred rapidly at room temperature for 1 h. The reaction was monitored by ^{1}H-NMR spectroscopy, which indicated 58 μmol of cyclohexane was produced in 1 h (TOF = 1.3 mol C_6H_6·mol Zr·h^{-1}).

Computational Methods. Density functional theory (DFT)-based simulations were performed with the CP2K/Quickstep package using a hybrid Gaussian and plane-wave method (5). A double-quality Gaussian basis set plus polarization (DZVP) was used for the Zr atom and a triple-quality Gaussian basis set plus polarization (TZVP) was used for all the other atoms. The Goedecker-Teter-Hutter pseudopotentials (6), together with a 400 Rydberg plane-wave cutoff, were used to expand the densities obtained with the Perdew-Burke-Ernzerhof (7) exchange-correlation density functional, and van der Waals forces were taken into account with the Grimme D3 method (8). Only the gamma point was considered in a supercell approach. Periodic boundary conditions were applied in all directions of space. The transition states were searched with the "distinguished reaction coordinate procedure" along the emerging bonds.

Surface model. The alumina (*110*) surface (9, 10) was constructed using a slab model having a (2 × 2) surface unit cell with a 20-Å vacuum region between the slabs. A single adsorbate/catalyst molecule was placed on one side of the slab to reduce lateral interactions. The sulfated alumina surface was constructed by determining the lowest energy structures for adsorption of H_2SO_4 molecules on the alumina (*110*) surface. The bottom exposed surface was partially hydroxylated (hydroxyl coverage θ_{OH} = 11.8 OH nm^{-2}), whereas the upper surface was sulfated as follows. Briefly, the adsorption of H_2SO_4 molecules was modeled as an exchange/condensation reaction with the hydroxyl groups of the partially dehydroxylated alumina surface, where θ_{OH} = 11.8 nm^{-2}. The most stable sulfated surface was then subjected to a dehydration process at 550 °C, as in the actual AlS synthesis, yielding a surface suitable for the chemisorption process with the sulfate species coverage θ_{H2SO4} = 3.0 H_2SO_4 nm^{-2}, whereas the hydroxyl coverage θ_{OH} = 4.4 OH nm^{-2}. The two principal sulfate species found on the alumina surface are shown in Fig. S2. $\mathbf{S_A}$ formation involves a double-exchange/condensation reaction with the surface and does not have an acidic proton, whereas $\mathbf{S_B}$ arises from a single exchange/condensation reaction with the surface and, hence, preserves one acidic proton that in turn gives to the Al–O surface groups via an acid/base exchange process. A vibrational frequency analysis, performed on the $\mathbf{B/S_A}$ structure is particularly informative. Interaction of the Zr center with the sulfate S = O fragment induces a downward frequency shift of the O = S = O asymmetric stretching mode of ∼70 cm^{-1} (from 1,308 cm^{-1} to 1,240 cm^{-1}), in excellent accord with experimental IR spectroscopic results obtained for analogous zirconocene chemisorptions on ZrS (11).

Benzene hydrogenation cycle. For the benzene hydrogenation cycle catalyzed by organozirconium complexes adsorbed on sulfated alumina, transition states were searched using the "distinguished reaction coordinate procedure" along the emerging bonds. In particular, we followed the energetic trends (*i*) during the approach of the benzene to the catalytic site (benzene coordination step), constraining the $Zr–Be_{centroid}$ distance; (*ii*) during the hydride transfer (step **I**), constraining the emerging C–H bond; (*iii*) during the approach of the H_2 molecule (H_2 activation, step **II**), constraining the Zr–H distance; and (*iv*) during the Zr–C hydrogenolysis (step **III**), constraining the H–H distance. We computed steps **I**, **II**, and **III** transition states only within the second hydrogenation subcycle as representative of all hydrogenation subcycles. Thermal and entropic contributions were evaluated only on the first hydrogenation subcycle, computing the parent naked $Cp^*ZrMe_2^+$ catalyst system by performing the geometry optimization, followed by the frequency calculation as implemented in the Gaussian09 code (12). In these cases, calculations were performed at the level of the B3LYP formalism. The effective core potential of Hay and Wadt (13), which explicitly treats 4s and 4p electrons and a basis set contracted as [4s, 4p, 4d], was used for the Zr atom. The standard all-electron 6–31G** basis was used for the remaining atoms (14, 15). Molecular geometry optimization of stationary points used analytical gradient techniques. Then, the thermal and entropic corrections were "appended" to the benzene hydrogenation energy profile, evaluated on the surface using the CP2K code. As expected, the principal modifications of the energy profile involve the association processes (benzene coordination and H_2 coordination) and the product release. In particular, entropic contributions destabilize the coordination events by about 10–13 kcal/mol, and, vice versa, the product release is stabilized by an entropic contribution (−12 kcal/mol). For all other steps, the entropic contributions account for only slight changes in energy (1–3 kcal/mol).

X-ray Absorption Spectroscopy (XAS) Measurements. Zr K-edge (17.998 keV) EXAFS and XANES data were collected on the insertion-device beam line of the Materials Research Collaborative Access Team (MRCAT, Sector 10 ID) at the Advanced Photon Source, Argonne National Laboratory. A cryogenically cooled double-crystal Si (111) monochromator was used in conjunction with an uncoated glass mirror to minimize the presence of harmonics. The monochromator was scanned continuously during the measurements with data points integrated over 0.5 eV for 0.07 s per data point. Complete XANES and EXAFS spectra were obtained in about 120 s under N_2 at 25 °C (16). Measurements were made in the transmission mode with the ionization chambers optimized for the maximum current with linear response (∼10^{10} photons detected s^{-1}) using gas mixtures (75% N_2 + 25% Ar) to give 10% absorption in the incident X-ray detector and 35% absorption (Ar) in the transmission X-ray detector. A Zr foil spectrum was acquired simultaneously with each measurement for energy calibration. Catalyst samples were pressed into a cylindrical holder of ca. 5 mm diameter with a thickness chosen to give a total absorbance (μx) of about 2.0.

X-Ray Adsorption Fine Structure Spectroscopy Data Analysis. The Zr–C extended X-ray adsorption fine structure spectroscopy (EXAFS) coordination numbers and bond distances were obtained by a least-squares fit in R space of the k^2-weighted data using the phase and amplitude functions calculated with FEFF. Both the magnitude and imaginary parts of the Fourier transform were fit. The presence of multiple scatters of similar backscattering phase and amplitude can, in principle, make it difficult to resolve them. The approach taken here was to isolate separate structural contributions by first synthesizing structurally similar molecules and analyzing the EXAFS spectrum of each. As discussed in the text, there is excellent agreement between the single crystal diffraction–determined structures of these model complexes and the EXAFS-derived structures of the neat powders in terms of coordination numbers and bond distances. To resolve individual scattering contributions, simplified Zr compounds were prepared to isolate scattering from this particular structural feature. For example, subtracting the structurally similar Cp_2ZrH_2 spectrum from the $Cp_2Zr(CH_3)_2$ spectrum (Fig. S3) is used to derive two $Zr–CH_3$ contributions, which are at a different Zr-ligand distance and can be separated by Fourier filtering. Once the separate $Zr–CH_3$ features are fit, $Cp_2Zr(CH_3)_2$ can be fit using a two-shell fit of the Zr–Cp and $Zr–CH_3$ contributions (which are now known) to fit the total EXAFS spectrum. These fits are in good agreement with the number of Cp carbons (i.e., 10) and the Zr–C bond distance, which is very similar to that of Cp_2ZrH_2, as assumed. These values are accurate within the limits of the XAS technique, e.g., about 10% in N. EXAFS refinement data are summarized in Table 2. The same difference approach was taken to fit the binding of the benzene substrate. The structure of the Cp^*ZrMe_3/sulfated alumina was subtracted from that of Cp^*ZrMe_3/sulfated alumina with added benzene (Fig. S4). The difference represents the coordination of benzene, and all other overlapping structural features are absent in the spectra. The differences in the disorder occur from the structural disorder in the different structural groups. The Cp rings typically have slightly different Zr–C bonds, whereas the 2 Zr–Me likely are more similar. Thus, the disorder terms will be slightly different. The most recent data have delta sigma squared (DSS) values, which are slightly different but within the normal range. Fits using slightly different DSS values (0.001–0.002) do not lead to different fit values within the normal errors of N. The E_0 fitting term is highly correlated with the bond distance (R). A change in any bond distance of 2.27 (Zr–Me) to 2.58 (Zr–Cp) Å will give these large changes in E_0. The E_0 in the EXAFS fit does not represent a change in the X-ray absorption near-edge structure edge energy, which is small (<1 eV) for all samples. Analysis was performed using WinXAS 3.1 software. The absorption spectra were normalized using a linear polynomial for the pre-edge region and a third-order polynomial for the post-edge region. Background subtraction was performed using a cubic spline with five nodes to about 14 $Å^{-1}$.

1. Morcombe CR, Zilm KW (2003) Chemical shift referencing in MAS solid state NMR. *J Magn Reson* 162(2):479–486.
2. Wailes P-C, Weigold H, Bell A-P (1972) Insertion reactions of dicyclopentadienyldimethylzirconium and related cyclopentadienyl compounds with sulfur-dioxide and nitric-oxide. *J Organomet Chem* 34(1):155–164.
3. Wolczanski P-T, Bercaw J-E (1982) Alkyl and hydride derivatives of (pentamethylcyclopentadienyl)zirconium(IV). *Organometallics* 1(6):793–799.
4. Williams L-A, Marks T-J (2009) Chemisorption pathways and catalytic olefin polymerization properties of group 4 mono- and binuclear constrained geometry complexes on highly acidic sulfated alumina. *Organometallics* 28(7):2053–2061.
5. The CP2K Developers Group.www.cp2k.org.
6. Goedecker S, Teter M, Hutter J (1996) Separable dual-space Gaussian pseudopotentials. *Phys Rev B Condens Matter* 54(3):1703–1710.
7. Perdew J-P, Burke K, Ernzerhof M (1996) Generalized gradient approximation made simple. *Phys Rev Lett* 77(18):3865–3868.
8. Grimme S, Antony J, Ehrlich S, Krieg H (2010) A consistent and accurate ab initio parametrization of density functional dispersion correction (DFT-D) for the 94 elements H-Pu. *J Chem Phys* 132(15):154104.
9. Motta A, Fragaà IL, Marks T-J (2008) Links between single-site heterogeneous and homogeneous catalysis. DFT analysis of pathways for organozirconium catalyst chemisorptive activation and olefin polymerization on γ-alumina. *J Am Chem Soc* 130 (49):16533–16546.
10. Digne M, Sautet P, Raybaud P, Euzen P, Toulhoat H (2004) Use of DFT to achieve a rational understanding of acid-basic properties of gamma-alumina surfaces. *J Catal* 226(1):54–68.
11. Nicholas C-P, Ahn H-S, Marks T-J (2003) Synthesis, spectroscopy, and catalytic properties of cationic organozirconium adsorbates on "super acidic" sulfated alumina. "Single-site" heterogeneous catalysts with virtually 100 active sites. *J Am Chem Soc* 125(14): 4325–4331.
12. Frisch M-J, et al. (2009) Gaussian 09, Revision A.1 (Gaussian, Inc., Wallingford CT).
13. Hay P-J, Wadt W-R (1985) Ab initio effective core potentials for molecular malculations. Potentials for K to Au including the outermost core orbitals. *J Chem Phys* 82(1):299–310.
14. Francl M-M, et al. (1982) Self-consistent molecular-orbital methods. 23. A polarization-type basis set for 2nd-row elements. *J Chem Phys* 77(7):3654–3665.
15. Hehre W-J, Ditchfie R, Pople J-A (1972) Self-consistent molecular-orbital methods.12. Further extensions of Gaussian-type basis sets for use in molecular-orbital studies of organic-molecules. *J Chem Phys* 56(5):2257–2261.
16. Castagnola N-B, Kropf A-J, Marshall C-L (2005) Studies of Cu-ZSM-5 by X-ray absorption spectroscopy and its application for the oxidation of benzene to phenol by air. *Appl Catal A* 290(1–2):110–122.

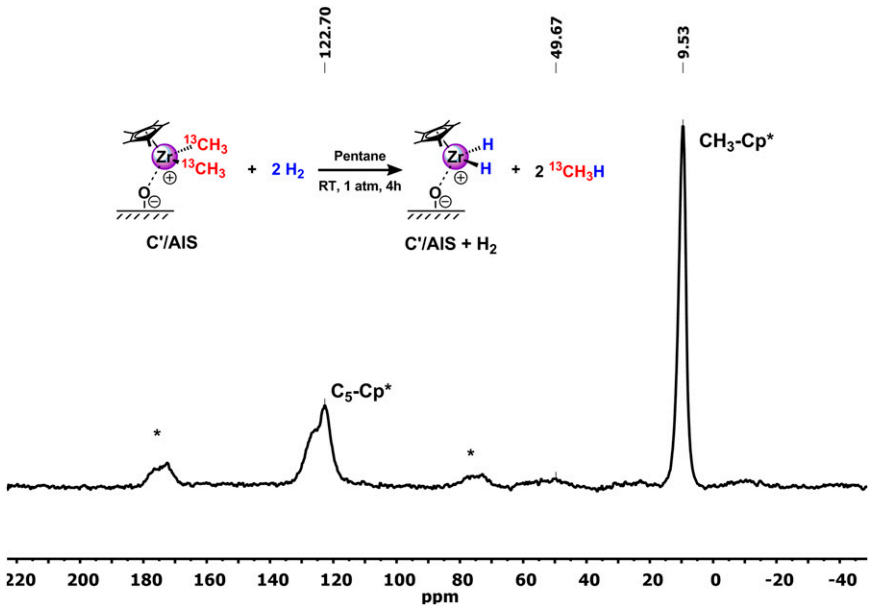

Fig. S1. Solid-state ^{13}C-NMR studies of hydrogenolyzed organozirconium complex on sulfated aluminum oxide. ^{13}C-CPMAS-NMR spectrum (100 MHz, 16K scans; repetition time, 5 s; contact time, 2 ms; spinning speed, 5 kHz) of Cp*Zr($^{13}CH_3$)$_3$ + H_2 (**C'/AlS** + H_2). *Rotational sidebands.

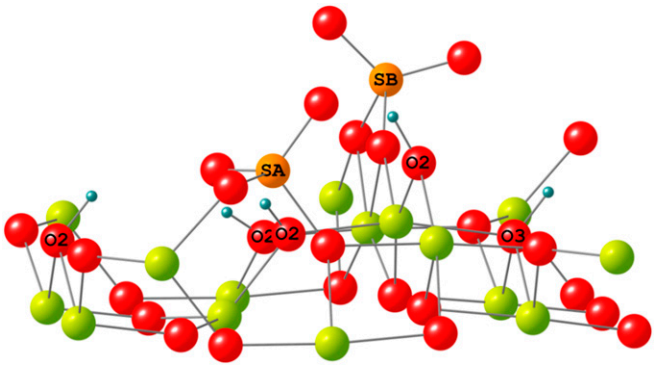

Fig. S2. Structures of sulfate species $\mathbf{S_A}$ and $\mathbf{S_B}$ on the DFT-modeled AlS surface. Al, yellow-green; H, blue; O, red; S, orange.

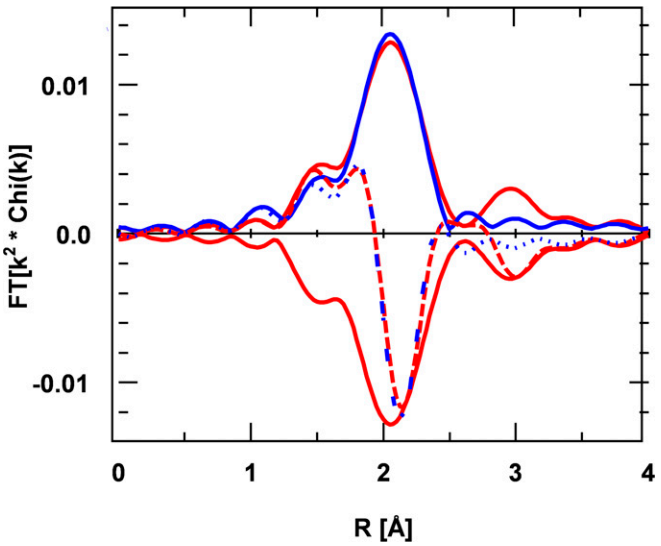

Fig. S3. k^2-weighted Fourier transform (FT) of the Zr K-edge EXAFS of Cp_2ZrMe_2 (complex **B**). Red, Δk = 3.2–11.6 $Å^{-1}$ data; blue, fit for ΔR = 1.5–2.6 Å; solid line, FT magnitude; dotted line, FT imaginary part.

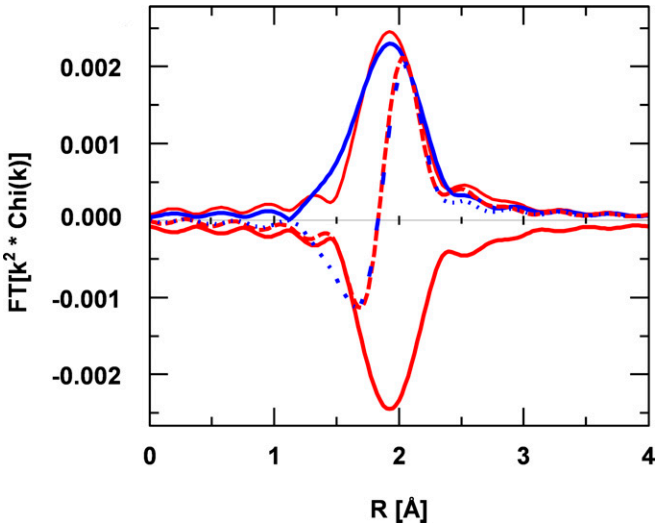

Fig. S4. k^2-weighted Fourier transform (FT) of the Zr K-edge EXAFS of $\mathbf{C{\cdot}C_6H_6/AlS}$ − $\mathbf{C{\cdot}C_6H_6/AlS/H_2}$. Red, Δk = 3.2–11.6 $Å^{-1}$ data; blue, fit ΔR = 1.5–2.6 Å; ($N_{Zr\text{-}Bz}$ = 1.6 at 2.36 Å) for ΔR = 1.5–2.6 Å; solid line, FT magnitude; dotted line, FT imaginary part.